*metals*

MDPI

*Article*

# Structural and Magnetic Properties of P Microalloyed $Fe_{76}Cu_{0.8}Nb_{2.2}B_9Si_{12}$ Alloys

**Jiawei Li [1,2], Qian Ding [1,3], Changjiu Wang [1], Aina He [1,2,*], Yaqiang Dong [1,2] and Deren Li [4,*]**

[1] CAS Key Laboratory of Magnetic Materials and Devices and Zhejiang Province Key Laboratory of Magnetic Materials and Application Technology, Ningbo Institute of Materials Technology & Engineering, Chinese Academy of Sciences, Ningbo 315201, China; lijw@nimte.ac.cn (J.L.); dingqian@nimte.ac.cn (Q.D.); wangchangjiu@nimte.ac.cn (C.W.); dongyq@nimte.ac.cn (Y.D.)
[2] University of Chinese Academy of Sciences, Beijing 100049, China
[3] Faculty of Materials Science and Chemical Engineering, Ningbo University, Ningbo 315211, China
[4] School of Electrical Engineering, Beijing Jiaotong University, Beijing 100044, China
* Correspondence: hean@nimte.ac.cn (A.H.); derenli@bjtu.edu.cn (D.L.); Tel.: +86-574-87617212 (A.H.); +86-10-51684316 (D.L.)

**Abstract:** The development of Fe-based nanocrystalline alloys with high saturation magnetization ($B_s$), excellent magnetic softness and good manufacturability is highly desirable. Here, the effect of substituting 1 at% P for B and Si on the thermal stability, microstructure and magnetic properties of $Fe_{76}Cu_{0.8}Nb_{2.2}B_9Si_{12}$ alloy has been studied in detail. It was found that replacing B with P effectively reduces the coercivity ($H_c$) of the alloy without deteriorating the $B_s$ and permeability ($\mu$). However, replacing Si with P has little effect on the $H_c$ and $B_s$, yet significantly reduces the $\mu$. The variation in the magnetic properties can be well understood from the evolution of the microstructure and magnetic anisotropy induced by P microalloying. The $Fe_{76}Cu_{0.8}Nb_{2.2}B_8Si_{12}P_1$ alloy with a good processing window, a high $B_s$ of 1.41 T, a great $\mu$ of 29,000 at 1 kHz and a low $H_c$ of 0.6 A/m is suitable for high-power electronic devices.

**Keywords:** nanocrystalline alloys; microstructure; magnetic properties; microalloying; magnetic anisotropy

check for updates

**Citation:** Li, J.; Ding, Q.; Wang, C.; He, A.; Dong, Y.; Li, D. Structural and Magnetic Properties of P Microalloyed $Fe_{76}Cu_{0.8}Nb_{2.2}B_9Si_{12}$ Alloys. *Metals* **2021**, *11*, 1110. https://doi.org/10.3390/met11071110

Academic Editor: Imre Bakonyi

Received: 14 June 2021
Accepted: 8 July 2021
Published: 12 July 2021

**Publisher's Note:** MDPI stays neutral with regard to jurisdictional claims in published maps and institutional affiliations.

**Copyright:** © 2021 by the authors. Licensee MDPI, Basel, Switzerland. This article is an open access article distributed under the terms and conditions of the Creative Commons Attribution (CC BY) license (https://creativecommons.org/licenses/by/4.0/).

## 1. Introduction

Fe-Si-B-Nb-Cu nanocrystalline alloys first, demonstrated by Yoshizawa et al. in 1988 [1], have been the most widely studied and used nanocrystalline soft magnetic alloys. The nanocrystalline soft magnetic alloys have an amorphous/nanocrystalline dual-phase structure, comprising $\alpha$-Fe(Si) crystallites of less than 20 nm in diameter, uniformly embedded in a residual amorphous matrix that is approximately 1–2 nm thick [2–4]. This structure possesses large magnetization, small magnetocrystalline anisotropy and low magnetostrictive coefficient, which makes the Fe-Si-B-Nb-Cu nanocrystalline alloys present high permeability ($\mu$) and ultra-low coercivity ($H_c$) values [5–7]. However, the Fe-Si-B-Nb-Cu alloys currently in commercial use (named Finemet, with a typical composition of $Fe_{73.5}Si_{13.5}B_9Nb_3Cu_1$) have a low saturation magnetization ($B_s$) of around 1.24 T, which struggles to meet the development needs of the miniaturization and high power of electronic devices.

Increasing the quantity of Fe and Co elements is the most effective way to increase the $B_s$ of Fe-based nanocrystalline alloys [8–11]. In addition, reducing the content of non-magnetic metalloids [12], large early transition metals (Nb, Mo, Zr, etc.) [13–16] and post-transition metals such as Cu [17,18] is also beneficial to improve $B_s$. However, a high content of ferromagnetic elements usually leads to an increase in the magnetic anisotropy and a decrease in the amorphous-forming ability, which would deteriorate the soft magnetic properties of Fe-based nanocrystalline alloys [6,13,19]. Several studies have attempted to increase $B_s$ without degrading the soft magnetic properties and amorphous-forming

ability of the nanocrystalline alloys with high Fe content by microalloying P [20,21], Al [22], Nb [10,23], Sn [24], Mo [25–27] and C [28]. Among them, P has less negative impact on $B_s$ than early transition metals such as Nb [29], and is more effective than metalloids such as B [30] and Si [31] in inhibiting the growth of α-Fe(Si) grains.

Recently, we fabricated an $Fe_{76}Cu_1Nb_2B_8Si_{13}$ nanocrystalline alloy with good soft magnetic properties and manufacturability [10,32]. However, the low $\mu$ limits its application. It was found that the addition of Mn effectively enhances the high-frequency permeability of the alloy, but reduces $B_s$, and requires a harsh rapid heating annealing process [33]. In addition, P microalloying also improves the $\mu$ of the alloy. However, the optimal annealing temperature range for this P-doped alloy is narrow and the corresponding annealing time is short (10 min) [21]. Therefore, the manufacturability of these alloys needs to be further improved for large-scale production.

It was reported that the optimized Cu content required for nanocrystalline alloys with high Fe content to obtain the highest $\mu$ is about 0.6 at% [18]. Based on this work, we have recently optimized the composition of $Fe_{76}Cu_1Nb_2B_8Si_{13}$ alloy, and unexpectedly found that the annealing window of $Fe_{76}Cu_{0.8}Nb_{2.2}B_9Si_{12}$ alloy is very wide, that is, the difference between the first and second onset crystallization temperatures is as high as 207 °C and the annealing time can be as long as 1 h or more. Unfortunately, although the $\mu$ of the $Fe_{76}Cu_{0.8}Nb_{2.2}B_9Si_{12}$ alloy is as high as 29,000 at 1 kHz, the coercivity $H_c$ is larger than 3 A/m, which would lead to high hysteresis loss [3].

The aim of this work is to evaluate the effectiveness of P microalloying in reducing the $H_c$ without decreasing the $B_s$ and $\mu$ of the $Fe_{76}Cu_{0.8}Nb_{2.2}B_9Si_{12}$ alloy, and to reveal why slight changes in P, B and Si contents have a significant impact on the soft magnetic properties of the alloy. It was found that although the addition of 1 at% P significantly reduces the annealing temperature range of the alloy, it still has greater manufacturability than that of the Mn-doped and P-doped $Fe_{76}Cu_1Nb_2B_8Si_{13}$ alloys. In addition, substituting 1 at% P for B and Si has significantly different effects on the microstructure and soft magnetic properties of the alloys. We have explored this interesting phenomenon by studying the evolution of microstructure and magnetic anisotropy. The developed $Fe_{76}Cu_{0.8}Nb_{2.2}B_8Si_{12}P_1$ alloy exhibits a high $B_s$ of 1.41 T, a great $\mu$ of 29,000 at 1 kHz and a low $H_c$ of 0.6 A/m, making it suitable for high-power electronic devices.

## 2. Experimental

Master alloy ingots with nominal compositions of $Fe_{76}Cu_{0.8}Nb_{2.2}B_9Si_{12}$, $Fe_{76}Cu_{0.8}Nb_{2.2}B_8Si_{12}P_1$ and $Fe_{76}Cu_{0.8}Nb_{2.2}B_9Si_{11}P_1$ (at%) were prepared by induction melting with highly pure raw materials of Fe (99.99 wt%), Cu (99.99 wt%), Nb (99.99 wt%), B (99.95 wt%), Si (99.99 wt%) and pre-alloyed $Fe_3P$ (99.99 wt%) under a pure argon atmosphere. Melt-spun ribbons with a thickness of approximately 27–30 μm and a width about 1 mm were produced by a single-roller melt-spinning method with a copper roller speed of 35 m/s in an argon atmosphere. Nanocrystalline ribbons were prepared by annealing the melt-spun ribbons at 510–590 °C for 60 min in an isothermal tube annealing furnace (Shanghai Y-feng electrical furnace Co., Ltd., Shanghai, China) under a vacuum degree of $5 \times 10^{-3}$ Pa followed by water quenching.

Thermal parameters, including the onset crystallization temperatures of the melt-spun ribbons, were evaluated by differential scanning calorimetry (DSC, NETZSCH 404C, Selb, Germany) at a heating rate of 0.67 °C/s under high-purity argon flow. Magnetic properties such as $B_s$, $H_c$ and $\mu$ were measured by a vibrating sample magnetometer (VSM, Lakeshore 7410, Columbus, OH, USA) under a maximum applied field of 800 kA/m, a DC B-H loop tracer (EXPH-100, Riken Deshi Co., Ltd., Saitama, Japan) under a maximum applied field of 800 A/m and an HP4294A impedance analyzer with a frequency from 1 kHz to 110 MHz in a field of 1 A/m, respectively. The amorphous structure of the melt-spun ribbons and the precipitates of the annealed ribbons were identified by X-ray diffraction (XRD, Bruker D8 Advance, Karlsruhe, Germany) with Cu-Kα radiation and transmission electron microscopy (TEM, TF20, Hillsboro, OR, USA).

## 3. Results and Discussion

Figure 1 shows the XRD patterns of the melt-spun $Fe_{76}Cu_{0.8}Nb_{2.2}B_9Si_{12}$, $Fe_{76}Cu_{0.8}Nb_{2.2}B_8Si_{12}P_1$ and $Fe_{76}Cu_{0.8}Nb_{2.2}B_9Si_{11}P_1$ ribbons. For convenience, we abbreviate the chemical formulas of the above alloys as $B_9Si_{12}$, $B_8Si_{12}P_1$ and $B_9Si_{11}P_1$, respectively. The melt-spun ribbons have typical diffraction peaks of an amorphous structure, that is, broad diffuse reflection peaks, and no sharp crystal diffraction peaks can be seen. The fully amorphous structure of the 30 μm thick ribbons indicates the good amorphous-forming ability of the present alloys, which is beneficial to obtain homogeneous and fine nanocrystalline grains [2].

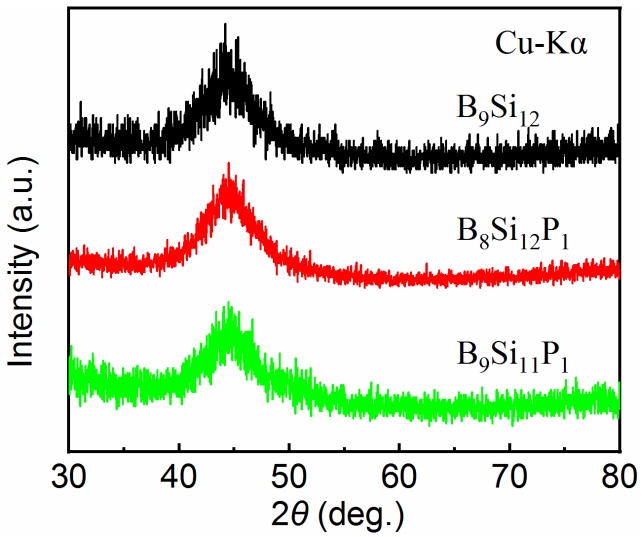



**Figure 1.** XRD patterns of melt-spun $Fe_{76}Cu_{0.8}Nb_{2.2}B_9Si_{12}$ ($B_9Si_{12}$), $Fe_{76}Cu_{0.8}Nb_{2.2}B_8Si_{12}P_1$ ($B_8Si_{12}P_1$) and $Fe_{76}Cu_{0.8}Nb_{2.2}B_9Si_{11}P_1$ ($B_9Si_{11}P_1$) ribbons.

Figure 2 shows the DSC curves of the melt-spun $B_9Si_{12}$, $B_8Si_{12}P_1$ and $B_9Si_{11}P_1$ ribbons. All ribbons have two distinct exothermic peaks, and the first and second crystallization peaks represent the precipitation of α-Fe(Si) and Fe-boride phases, respectively [21,33]. The difference between the first and second onset crystallization temperatures ($\Delta T = T_{x2} - T_{x1}$) of the $B_9Si_{12}$ ribbon is as high as 207 °C, which is much greater than that of the previously developed $Fe_{76}Cu_1Nb_2B_8Si_{13}$ (163 °C) alloy [10]. It should be pointed out that the DSC results of the ribbons obtained by re-preparing the master alloy all confirm that the $\Delta T$ of $B_9Si_{12}$ is 207 ± 2 °C. The large $\Delta T$ can extend the processing window, so that single α-Fe(Si) nanocrystalline grains can be formed in a wider annealing temperature range and a longer annealing time [2]. It is clearly seen that the addition of 1 at% P has little effect on $T_{x1}$, whereas it significantly decreases $T_{x2}$, resulting in the $\Delta T$ of $B_8Si_{12}P_1$ and $B_9Si_{11}P_1$ alloys decreasing to 158 °C and 149 °C, respectively. The phenomenon that P doping leads to a decrease in $T_{x2}$ is consistent with previous results [13,20,21]. It is reasonable to deduce that since the mixing enthalpy of P and B is positive (0.5 kJ/mol [34]), when P and B are excluded from the α-Fe(Si) grains during crystallization, the mutual repulsion of P and B may promote the precipitation of Fe-B phase, resulting in the decrease in $T_{x2}$. Nevertheless, the $\Delta T$ of $B_8Si_{12}P_1$ is still larger than that of typical Finemet alloys (140 °C) [35], and recently developed $Fe_{73}Cu_1Nb_2B_8Si_{13}Mn_3$ (149 °C) [33], $Fe_{76}Cu_1Nb_2B_7Si_{13}P_1$ (152 °C) and $Fe_{76}Cu_1Nb_{1.5}B_8Si_{13}Mo_{0.5}$ (151 °C) alloys [21], implying the good annealing process window of the present alloys.

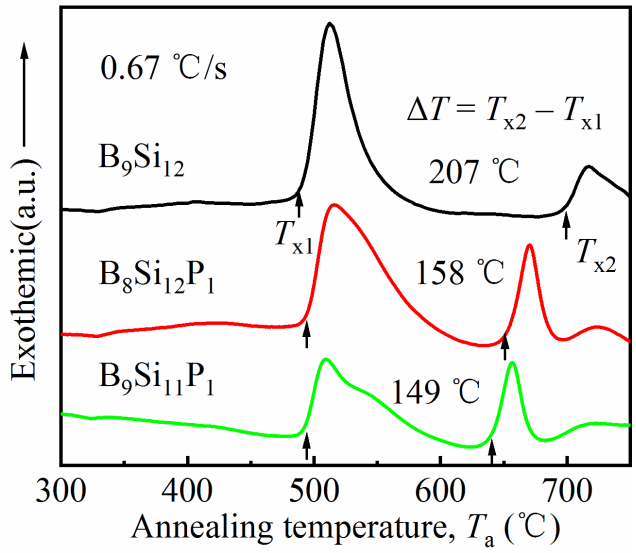



**Figure 2.** DSC curves of melt-spun $B_9Si_{12}$, $B_8Si_{12}P_1$ and $B_9Si_{11}P_1$ ribbons at a heating rate of 0.67 °C/s. $T_{x1}$ and $T_{x2}$ denote the first and second onset crystallization temperatures, respectively. $\Delta T = T_{x2} - T_{x1}$, reflecting the annealing temperature range for obtaining single fine nanocrystalline grains.

In order to obtain homogeneous and fine α-Fe(Si) grains, the annealing temperature was selected from 510–590 °C based on the DSC results [2,3]. Figure 3 shows the $H_c$ of the melt-spun $B_9Si_{12}$, $B_8Si_{12}P_1$ and $B_9Si_{11}P_1$ ribbons as a function of annealing temperature. The $H_c$ was obtained by testing the hysteresis loop of the ribbons with a length of about 70 mm by a DC B-H loop tracer. As the annealing temperature rises from 510 to 570 °C, the $H_c$ of $B_9Si_{12}$ and $B_9Si_{11}P_1$ increases from 1.7 to 3.6 A/m and 2.1 to 2.5 A/m, respectively, whereas the $H_c$ of $B_8Si_{12}P_1$ first decreases from 2.0 to 0.6 A/m and then increases to 1.8 A/m. The reduced $H_c$ of $B_8Si_{12}P_1$ with increasing temperature may be related to the stable and fine α-Fe(Si) grains, as well as the increased crystalline volume fraction [2]. However, an excessively high annealing temperature may cause the grains to grow and precipitate Fe-boride phase, thus the $H_c$ increases. The relationship between structure and $H_c$ will be discussed in detail below. Therefore, substituting 1 at% P for Si has limited effect in reducing $H_c$, while substituting 1 at% P for B can effectively reduce the $H_c$ to the level of the commercial Finemet alloys [35]. However, when the annealing temperature increases to 590 °C, the $H_c$ of $B_9Si_{12}$ decreases slightly. On the contrary, the $H_c$ of $B_8Si_{12}P_1$ and $B_9Si_{11}P_1$ increases significantly. This result may originate from the reduced $\Delta T$ of the P-doped alloys, which easily precipitate Fe-boride compounds with high magnetocrystalline anisotropy during high-temperature and long-term annealing [3]. Nevertheless, the $H_c$ of $B_8Si_{12}P_1$ in the annealing temperature range of 510–570 °C is less than 2 A/m, which is advantageous compared with the $B_9Si_{12}$ and $B_9Si_{11}P_1$ alloys.

Figure 4 shows the $\mu$ of the melt-spun $B_9Si_{12}$, $B_8Si_{12}P_1$ and $B_9Si_{11}P_1$ ribbons as a function of annealing temperature. The $\mu$ was obtained by measuring the magnetic spectrum of the 50 mm long ribbons by an HP4294A impedance analyzer in a field of 1 A/m. The $\mu$ of $B_9Si_{12}$ increases gradually with the increase in annealing temperature, reaching 29,000 at 590 °C. The $\mu$ of $B_8Si_{12}P_1$ and $B_9Si_{11}P_1$ first increases and then decreases with increasing annealing temperature. However, $B_8Si_{12}P_1$ has a $\mu$ comparable to that of $B_9Si_{12}$ in the temperature range of 510–570 °C, while the $\mu$ of $B_9Si_{11}P_1$ is very low, less than 18,000. Except for $B_8Si_{12}P_1$, the $\mu$ of $B_9Si_{12}$ and $B_9Si_{11}P_1$ does not change inversely to the $H_c$. Similar phenomena can also be found in other nanocrystalline alloy systems [22,36]. It is well known that the magnetoelastic anisotropy of Fe-Cu-Nb-B-Si nanocrystalline alloys is sensitive to Si content, which significantly affects the $\mu$ of the alloys. When the Si content is around 15 at%, the magnetoelastic anisotropy of the alloys is close to zero [36]. Moreover, a slight

change in Si content also has a remarkable effect on the $\mu$ of nanocrystalline alloys [36,37]. For example, in the Fe-Si-B-P-Cu system, the $\mu$ of alloys that differ only by 1 at% Si differs by more than 3000. Therefore, $B_9Si_{11}P_1$ with less Si content has a smaller $\mu$ than $B_9Si_{12}$ and $B_8Si_{12}P_1$, which may be related to the increased magnetoelastic anisotropy [3,36].

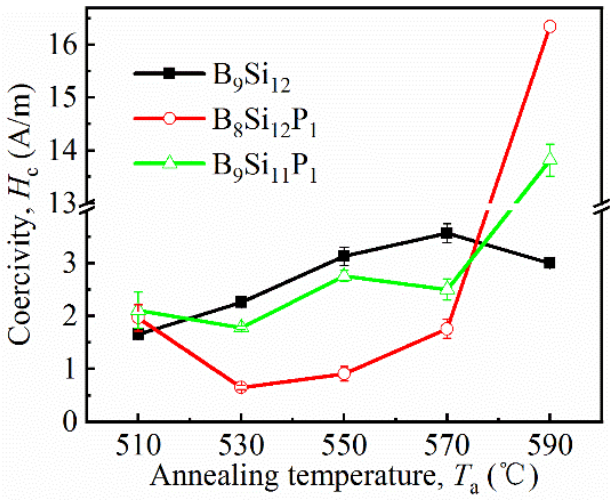



**Figure 3.** $H_c$ of $B_9Si_{12}$, $B_8Si_{12}P_1$ and $B_9Si_{11}P_1$ ribbons as a function of annealing temperature. The annealing time is 60 min.

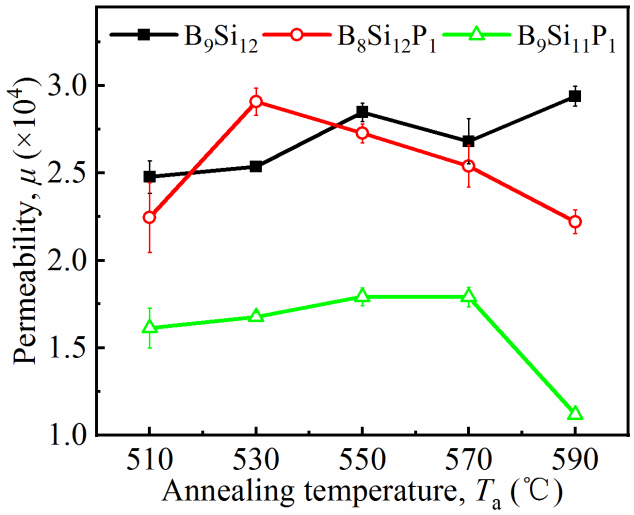



**Figure 4.** $\mu$ of $B_9Si_{12}$, $B_8Si_{12}P_1$ and $B_9Si_{11}P_1$ ribbons at 1 kHz as a function of annealing temperature. The annealing time is 60 min.

Figure 5 shows typical hysteresis loops of the $B_9Si_{12}$, $B_8Si_{12}P_1$ and $B_9Si_{11}P_1$ ribbons after annealing at 550 °C for 60 min. The $B_s$ of the samples (a total of eight 3 mm long ribbons) was obtained by a VSM at a maximum field strength of 800 kA/m. All samples show a slender hysteresis loop, and the curves have a high slope under a small applied magnetic field, typical characteristics of soft magnetic materials. The $B_s$ values of the annealed $B_9Si_{12}$, $B_8Si_{12}P_1$ and $B_9Si_{11}P_1$ ribbons are 1.36 T, 1.41 T and 1.42 T, respectively, implying that the substitution of 1 at % P for metalloids has little effect on the $B_s$ of the alloys. Therefore, the above results demonstrate the effectiveness of P microalloying in reducing the $H_c$ without decreasing the $B_s$ and $\mu$ of the $Fe_{76}Cu_{0.8}Nb_{2.2}B_9Si_{12}$ alloy. In addition, the annealing time can be over 60 min in the optimal temperature range of 510–570 °C, indicating the good annealing process window of the alloys. Compared with the previously reported $Fe_{76}Cu_1Nb_2B_8Si_{13}$ [10,32], $Fe_{76-x}Cu_1Nb_2B_8Si_{13}Mn_x$ [33], $Fe_{76}Cu_1Nb_2B_7Si_{13}P_1$

and $Fe_{76}Cu_1Nb_{1.5}B_8Si_{13}Mo_{0.5}$ alloys [21], the present $Fe_{76}Cu_{0.8}Nb_{2.2}B_8Si_{12}P_1$ alloy has better annealing processability and superior overall magnetic properties.

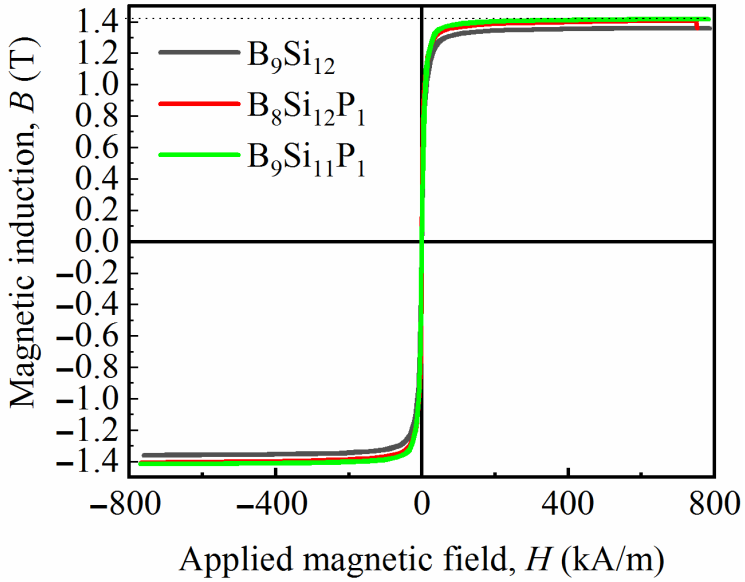



**Figure 5.** Typical hysteresis loops of $B_9Si_{12}$, $B_8Si_{12}P_1$ and $B_9Si_{11}P_1$ ribbons annealed at 550 °C for 60 min.

According to Herzer's random anisotropy model, the $H_c$ of nanocrystalline alloys is proportional to the sixth power of grain size for grain sizes below about 50 nm [36]. Thus, we investigated the influence of P microalloying on the $H_c$ of the alloys in terms of the variation in grain size and its distribution. Figure 6 shows the XRD patterns of the $B_9Si_{12}$, $B_8Si_{12}P_1$ and $B_9Si_{11}P_1$ ribbons annealed at 550 °C for 60 min. The XRD patterns show one main diffraction peak at about $2\theta = 45°$ and two sub-diffraction peaks at about $2\theta = 65°$ and 83°. The sharp diffraction peaks indicate that the annealed ribbons have undergone obvious crystallization, and only α-Fe(Si) grains are precipitated in the amorphous matrix. The full width at half maximum of the diffraction peaks of $B_8Si_{12}P_1$ (0.65°) is larger than that of $B_9Si_{12}$ (0.64°) and $B_9Si_{11}P_1$ (0.71°). The crystallite size can be calculated using the following equation: $L = K\lambda/(B\cos\theta)$, where $L$ is the linear dimension of crystallite, $K$ is the numerical constant (0.9), $\lambda$ is the wave-length of the incident X-ray, and $B$ is the full width at half maximum [38–40]. The crystallite sizes of $B_9Si_{12}$, $B_8Si_{12}P_1$ and $B_9Si_{11}P_1$ obtained from the XRD patterns are about 13 nm, 12 nm and 13 nm, respectively. Thus, $B_8Si_{12}P_1$ has the smallest grain size.

In order to further confirm the influence of P microalloying on the crystalline phase and its size and distribution, we observed the TEM micrographs, selected-area electron diffraction (SAED) and characteristic grain size distribution of the $B_9Si_{12}$, $B_8Si_{12}P_1$ and $B_9Si_{11}P_1$ ribbons annealed at 550 °C. As shown in Figure 7, all ribbons exhibit a typical nanocrystalline structure where α-Fe(Si) grains (confirmed by the SAED) are randomly embedded in the residual amorphous matrix, which is consistent with the XRD results. The α-Fe(Si) grains of $B_9Si_{12}$, $B_8Si_{12}P_1$ and $B_9Si_{11}P_1$ have an average size of approximately 12 nm, 11 nm and 12 nm, respectively. The XRD and TEM results indicate that substituting 1 at% P for B and Si is beneficial for reducing the size of α-Fe(Si) grains. In particular, the substitution of P for B is more beneficial to refine grain size than that of P for Si. Since the mixing enthalpies of the P-B atomic pair, P-Si atomic pair and Si-B atomic pair are 0.5 kJ/mol, −25.5 kJ/mol and −14 kJ/mol, respectively [34], the substitution of P for B effectively improved the negative mixing enthalpies of atomic pairs, which helps to inhibit long-range diffusion between atoms [41], making the grain size of $B_8Si_{12}P_1$ the smallest. In addition, the grain size of $B_8Si_{12}P_1$ is rarely above 22 nm and mainly distributed around

10 nm. Based on the random anisotropy model [36], the smaller the average grain size of α-Fe(Si) grains, the smaller the $H_c$. Therefore, the reduced grain size of $B_8Si_{12}P_1$ is the main factor for achieving the minimum $H_c$.

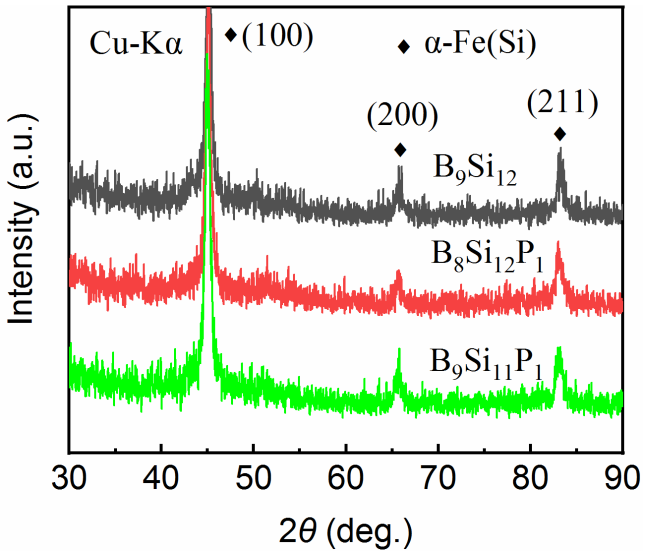



**Figure 6.** XRD patterns of $B_9Si_{12}$, $B_8Si_{12}P_1$ and $B_9Si_{11}P_1$ ribbons annealed at 550 °C for 60 min.

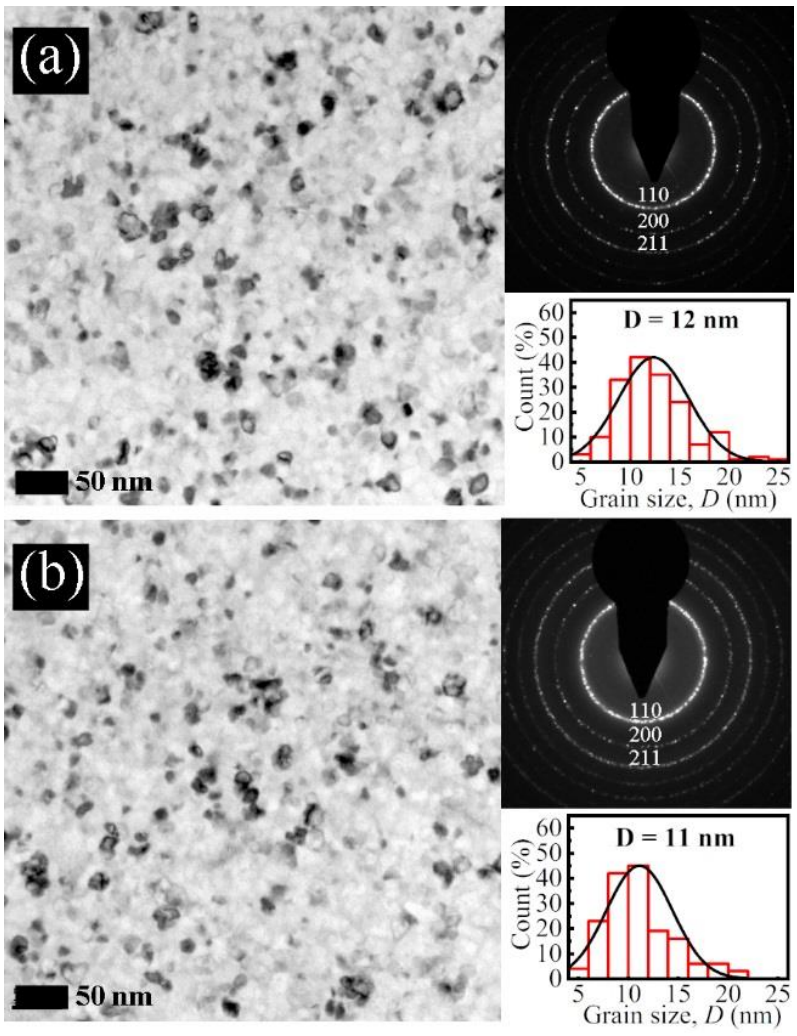



**Figure 7.** *Cont.*

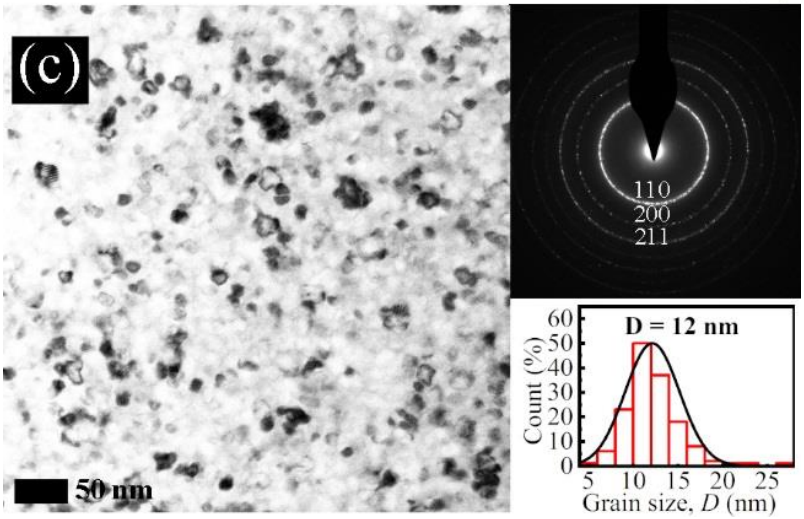



**Figure 7.** TEM micrographs, SAED and characteristic grain size distribution of (**a**) $B_9Si_{12}$, (**b**) $B_8Si_{12}P_1$ and (**c**) $B_9Si_{11}P_1$ ribbons annealed at 550 °C for 60 min.

## 4. Conclusions

The effect of P microalloying on the thermal stability, microstructure and magnetic properties of $Fe_{76}Cu_{0.8}Nb_{2.2}B_9Si_{12}$ alloy has been investigated. The slight changes in P, B and Si contents have little effect on $B_s$, but significantly affect the $H_c$ and $\mu$ of the alloy. Substituting 1 at% P for Si has a limited effect in reducing $H_c$, yet significantly reduces $\mu$. On the other hand, substituting 1 at% P for B can effectively decrease $H_c$ and keep $\mu$ basically unchanged. The $Fe_{76}Cu_{0.8}Nb_{2.2}B_8Si_{12}P_1$ alloy exhibits good annealing processability, a high $B_s$ of 1.41 T, a great $\mu$ of 29,000 at 1 kHz and a low $H_c$ of 0.6 A/m, which can be mainly attributed to the formation of more homogeneous and finer α-Fe(Si) grains.

**Author Contributions:** J.L.: Conceptualization, Data curation, Formal analysis, Funding acquisition, Investigation, Writing—original draft. Q.D.: Data curation, Investigation, Methodology, Software. C.W.: Investigation, Validation. A.H.: Funding acquisition, Writing—review and editing. Y.D.: Writing—review and editing, D.L.: Writing—review and editing. All authors have read and agreed to the published version of the manuscript.

**Funding:** This work was supported by National Natural Science Foundation of China (Grant No. 51771215), Public Projects of Zhejiang Province (Grant No. LGG20E010003), Ningbo Major Special Projects of the Plan "Science and Technology Innovation 2025" (Grant No. 2018B10084).

**Institutional Review Board Statement:** Not applicable.

**Informed Consent Statement:** Not applicable.

**Data Availability Statement:** The data presented in this study are available within the paper.

**Conflicts of Interest:** The authors declare no conflict of interest.

## References

1. Yoshizawa, Y.; Oguma, S.; Yamauchi, K. New Fe-based soft magnetic alloys composed of ultrafine grain structure. *J. Appl. Phys.* **1988**, *64*, 6044–6046. [CrossRef]
2. Willard, M.A.; Daniil, M. Chapter Four-Nanocrystalline Soft Magnetic Alloys Two Decades of Progress. In *Handbook of Magnetic Materials*; Buschow, K.H.J., Ed.; Elsevier: Amsterdam, The Netherlands, 2013; pp. 173–342.
3. Herzer, G. Modern soft magnets: Amorphous and nanocrystalline materials. *Acta Mater.* **2013**, *61*, 718–734. [CrossRef]
4. Li, F.C.; Liu, T.; Zhang, J.Y.; Shuang, S.; Wang, Q.; Wang, A.D.; Wang, J.G.; Yang, Y. Amorphous–nanocrystalline alloys: Fabrication, properties, and applications. *Mater. Today Adv.* **2019**, *4*, 100027. [CrossRef]
5. Azuma, D.; Ito, N.; Ohta, M. Recent progress in Fe-based amorphous and nanocrystalline soft magnetic materials. *J. Magn. Magn. Mater.* **2020**, *501*, 166373. [CrossRef]
6. Lopatina, E.; Soldatov, I.; Budinsky, V.; Marsilius, M.; Schultz, L.; Herzer, G.; Schafer, R. Surface crystallization and magnetic properties of $Fe_{84.3}Cu_{0.7}Si_4B_8P_3$ soft magnetic ribbons. *Acta Mater.* **2015**, *96*, 10–17.

7. Pradeep, K.G.; Herzer, G.; Choi, P.; Raabe, D. Atom probe tomography study of ultrahigh nanocrystallization rates in FeSiNbBCu soft magnetic amorphous alloys on rapid annealing. *Acta Mater.* **2014**, *68*, 295–309. [CrossRef]
8. Yoshizawa, Y.; Fujii, S.; Ping, D.H.; Ohnuma, M.; Hono, K. Magnetic properties of nanocrystalline Fe–Co–Cu–M–Si–B alloys (M: Nb, Zr). *Mater. Sci. Eng. A.* **2004**, *375–377*, 207–212. [CrossRef]
9. Yoshizawa, Y.; Fujii, S.; Ping, D.H.; Ohnuma, M.; Hono, K. Magnetic properties of nanocrystalline FeMCuNbSiB alloys (M: Co, Ni). *Scripta Mater.* **2003**, *48*, 863–868. [CrossRef]
10. Wan, F.P.; He, A.N.; Zhang, J.H.; Song, J.C.; Wang, A.D.; Chang, C.T.; Wang, X.M. Development of FeSiBNbCu Nanocrystalline Soft Magnetic Alloys with High $B_s$ and Good Manufacturability. *J. Electron. Mater.* **2016**, *45*, 4913–4918. [CrossRef]
11. Hasiak, M.; Fukunaga, H.; Ciurzyńska, W.H.; Yamashiro, Y. Effect of Co addition on microstructure and magnetic properties of $(Fe_{86-x}Co_x)$-Zr-B alloys. *Scripta Mater.* **2001**, *44*, 1465–1469. [CrossRef]
12. Li, H.; Wang, A.; Liu, T.; Chen, P.; He, A.; Li, Q.; Luan, J.; Liu, C.T. Design of Fe-based nanocrystalline alloys with superior magnetization and manufacturability. *Mater. Today* **2021**, *42*, 49–56. [CrossRef]
13. Shi, L.; Yao, K. Composition design for Fe-based soft magnetic amorphous and nanocrystalline alloys with high Fe content. *Mater. Des.* **2020**, *189*, 108511.
14. Makino, A.; Men, H.; Kubota, T.; Yubuta, K.; Inoue, A. FeSiBPCu Nanocrystalline Soft Magnetic Alloys with High $B_s$ of 1.9 Tesla Produced by Crystallizing Hetero-Amorphous Phase. *Mater. Trans.* **2009**, *50*, 204–209. [CrossRef]
15. Ohta, M.; Yoshizaw, Y. Magnetic properties of nanocrystalline $Fe_{82.65}Cu_{1.35}Si_xB_{16-x}$ alloys (x=0–7). *Appl. Phys. Lett.* **2007**, *91*, 062517.
16. Parsons, R.; Li, Z.; Suzuki, K. Nanocrystalline soft magnetic materials with a saturation magnetization greater than 2 T. *J. Magn. Magn. Mater.* **2019**, *485*, 180–186. [CrossRef]
17. Suzuki, K.; Parsons, R.; Zang, B.; Onodera, K.; Kishimoto, H.; Kato, A. Copper-free nanocrystalline soft magnetic materials with high saturation magnetization comparable to that of Si steel. *Appl. Phys. Lett.* **2017**, *110*, 012407. [CrossRef]
18. Ohnuma, M.; Hono, K.; Linderoth, S.; Pedersen, J.S.; Yoshizawa, Y.; Onodera, H. Small-angle neutron scattering and differential scanning calorimetry studies on the copper clustering stage of Fe-Si-B-Nb-Cu nanocrystalline alloys. *Acta Mater.* **2000**, *48*, 4783–4790. [CrossRef]
19. Kuhnt, M.; Xu, X.D.; Amalraj, M.; Kozikowski, P.; Pradeep, K.G.; Ohkubo, T.; Marsilius, M.; Strache, T.; Polak, C.; Ohnuma, M.; et al. The effect of Co addition on magnetic and structural properties of nanocrystalline (Fe,Co)-Si-B-P-Cu alloys. *J. Alloy Compd.* **2018**, *766*, 686–693. [CrossRef]
20. Wang, C.; Li, J.; Zhang, X.; Wu, J.; He, A.; Dong, Y. Effect of P microalloying on magnetic properties and structure of FeSiBNbCu nanocrystalline alloy. *J. Mater. Sci. Mater. Electron.* **2021**, *32*, 4177–4184. [CrossRef]
21. Xiao, H.Y.; Dong, Y.Q.; He, A.N.; Sun, H.; Wang, A.D.; Li, H.; Liu, L.; Liu, X.C.; Li, R.W. Magnetic softness and magnetization dynamics of FeSiBNbCu(P,Mo) nanocrystalline alloys with good high-frequency characterization. *J. Magn. Magn. Mater.* **2019**, *478*, 192–197. [CrossRef]
22. Wu, J.; He, A.; Dong, Y.; Li, J.; Lu, Y. Structural and magnetic characterization of Al microalloying nanocrystalline FeSiBNbCu alloys. *J. Magn. Magn. Mater.* **2020**, *505*, 166746. [CrossRef]
23. Wu, L.; Li, Y.; Yubuta, K.; He, A.; Zhang, Y.; Zhang, W. Optimization of the structure and soft magnetic properties of a $Fe_{87}B_{13}$ nanocrystalline alloy by additions of Cu and Nb. *J. Magn. Magn. Mater* **2020**, *497*, 166001. [CrossRef]
24. Ohta, M.; Chiwata, N. Development of Fe-based high $B_s$ nanocrystalline alloy powder. *J. Magn. Magn. Mater.* **2020**, *509*, 166838. [CrossRef]
25. Ohta, M.; Hasegawa, R.; Itabashi, H. Development of Block Cores Comprising High-$B_s$ Nanocrystalline Alloy Ribbon. *IEEE Trans. Magn.* **2018**, *54*, 1–4. [CrossRef]
26. Zanaeva, E.N.; Bazlov, A.I.; Milkova, D.A.; Churyumov, A.Y.; Inoue, A.; Tabachkova, N.Y.; Wang, F.; Kong, F.L.; Zhu, S.L. High-Frequency soft magnetic properties of Fe-Si-B-P-Mo-Cu amorphous and nanocrystalline alloys. *J. Non-Cryst Solids* **2019**, *526*, 119702. [CrossRef]
27. Jia, X.; Li, Y.; Xie, G.; Qi, T.; Zhang, W. Role of Mo addition on structure and magnetic properties of the $Fe_{85}Si_2B_8P_4Cu_1$ nanocrystalline alloy. *J. Non-Cryst Solids* **2018**, *481*, 590–593. [CrossRef]
28. Fan, X.; Zhang, T.; Jiang, M.; Yang, W.; Shen, B. Synthesis of novel FeSiBPCCu alloys with high amorphous forming ability and good soft magnetic properties. *J Non-Cryst Solids* **2019**, *503*, 36–43. [CrossRef]
29. Jia, Y.R.; Wang, Z.; Wang, F.; Han, Y.; Xie, Z.Y.; Li, L.J.; Zhang, L. Effect of P substitution for Nb on structure and soft magnetic properties of Si-rich FeCuNbSiB nanocrystalline alloys. *Mater. Sci. Eng. B* **2017**, *222*, 55–59. [CrossRef]
30. Butvinova, B.; Butvin, P.; Brzozka, K.; Kuzminski, M.; Mat'Ko, I.; Sr, P.S.; Chromcikova, M. Effects of surface crystallization and oxidation in nanocrystalline FeNbCuSiB(P) ribbons. *J. Magn. Magn. Mater.* **2017**, *424*, 233–237. [CrossRef]
31. Xu, J.; Yang, Y.; Yan, Q.; Hou, F.; Fan, C.; Wang, G.; Luo, T. Effects of the substitution of Si by P on crystallization behavior, soft magnetic properties and bending ductility of FeSiBCuPC alloys. *J. Alloy Compd.* **2019**, *816*, 152534. [CrossRef]
32. Xiao, H.; Wang, A.; Zhao, C.; He, A.; Zhang, G.; Li, H.; Li, R.-w.; Liu, X. Industrialization of a FeSiBNbCu nanocrystalline alloy with high Bs of 1.39 T and outstanding soft magnetic properties. *J. Mate. Sci. Mater. Electron.* **2018**, *29*, 19517–19523. [CrossRef]
33. Zhang, B.; Yang, F.; He, A.; Xiao, H.; Dong, Y.; Li, J.; Han, Y. Rapid Annealing Optimizing Magnetic Softness and Thermal Stability of Mn-Substituted Fe-Based Nanocrystalline Alloys. *Metals* **2021**, *11*, 20. [CrossRef]

34. Takeuchi, A.; Inoue, A. Classification of bulk metallic glasses by atomic size difference, heat of mixing and period of constituent elements and its application to characterization of the main alloying element. *Mater. Trans.* **2005**, *46*, 2817–2829. [CrossRef]
35. McHenry, M.E.; Willard, M.A.; Laughlin, D.E. Laughlin, Amorphous and nanocrystalline materials for applications as soft magnets. *Prog. Mater. Sci.* **1999**, *44*, 291–433. [CrossRef]
36. Herzer. Chapter 3-Nanocrystalline soft magnetic alloys. In *Handbook of Magnetic Materials*; Buschow, K.H.J., Ed.; Elsevier: Amsterdam, The Netherlands, 1997; pp. 415–462.
37. Makino, A. Nanocrystalline Soft Magnetic Fe-Si-B-P-Cu Alloys With High $B_s$ of 1.8–1.9T Contributable to Energy Saving. *IEEE Trans. Magn.* **2012**, *48*, 1331–1335. [CrossRef]
38. Cullity, B.D.; Stock, S.R. *Elements of X ray Diffraction*, 3rd ed.; Prentice Hall: Upper Saddle River, NJ, USA, 2001.
39. Mitra, R.; Ungár, T.; Weertman, J.R. A comparison of grain size measurements by X-ray diffraction and transmission electron microscopy methods. *Trans. Indian Inst. Met.* **2005**, *58*, 1125.
40. Gubicza, J. *X-ray Line Profile Analysis in Materials Science*; IGI-Global: Hershey, PA, USA, 2014; ISBN 978-1-4666-5852-3.
41. Inoue, A. Stabilization of metallic supercooled liquid and bulk amorphous alloys. *Acta Mater.* **2000**, *48*, 279–306. [CrossRef]